



## Aseismic slip and fault-normal strain along the central creeping section of the San Andreas fault

F. Rolandone,<sup>1</sup> R. Bürgmann,<sup>2</sup> D. C. Agnew,<sup>3</sup> I. A. Johanson,<sup>4</sup> D. C. Templeton,<sup>2</sup> M. A. d'Alessio,<sup>5</sup> S. J. Titus,<sup>6</sup> C. DeMets,<sup>6</sup> and B. Tikoff<sup>6</sup>

Received 23 April 2008; revised 13 June 2008; accepted 18 June 2008; published 22 July 2008.

[1] We use GPS data to measure the aseismic slip along the central San Andreas fault (CSAF) and the deformation across adjacent faults. Comparison of EDM and GPS data sets implies that, except for small-scale transients, the fault motion has been steady over the last 40 years. We add 42 new GPS velocities along the CSAF to constrain the regional strain distribution. Shear strain rates are less than  $0.083 \pm 0.010 \mu\text{strain/yr}$  adjacent to the creeping SAF, with 1–4.5 mm/yr of contraction across the Coast Ranges. Dislocation modeling of the data gives a deep, long-term slip rate of 31–35 mm/yr and a shallow (0–12 km) creep rate of 28 mm/yr along the central portion of the CSAF, consistent with surface creep measurements. The lower shallow slip rate may be due to the effect of partial locking along the CSAF or reflect reduced creep rates late in the earthquake cycle of the adjoining SAF rupture zones.

**Citation:** Rolandone, F., R. Bürgmann, D. C. Agnew, I. A. Johanson, D. C. Templeton, M. A. d'Alessio, S. J. Titus, C. DeMets, and B. Tikoff (2008), Aseismic slip and fault-normal strain along the central creeping section of the San Andreas fault, *Geophys. Res. Lett.*, 35, L14305, doi:10.1029/2008GL034437.

### 1. Introduction

[2] In central California, most of the relative motion between the Pacific plate and the Sierra Nevada Great Valley microplate is accommodated by strike slip along the San Andreas fault, with a small amount of convergent and transcurrent motion accommodated by active thrust faults and folds in the California Coast Ranges on both sides of the San Andreas. Uniquely, along 170 km of the central San Andreas fault (CSAF), the strike-slip motion occurs nearly aseismically as fault creep. The CSAF accommodates up to 32 mm/yr of its shallow slip as creep; the average surface creep rates increase gradually from each end to the center of the segment [Lisowski and Prescott, 1981; Titus *et al.*, 2006]. Each end of the CSAF is bounded by a transition region (around San Juan Bautista to the NW, and Parkfield to the SE) with moderate earthquakes and

reduced creep rates [Johanson and Bürgmann, 2005; Murray and Langbein, 2006]. The adjoining segments of the SAF show little to no creep, slipping mostly in large earthquakes, such as the 1906 San Francisco and 1857 Fort Tejon shocks. The central 60 km of the CSAF has had no earthquakes larger than magnitude 4 over the last 65 years.

[3] Microseismicity on the CSAF is shallower than 12 km, suggesting a transition to fully aseismic slip or ductile deformation at this depth. The microseismic events occur only in certain areas, and probably represent small asperities failing by stick slip on an otherwise creeping fault [Wesson *et al.*, 1973; Nadeau and McEvilly, 2004]. Previous geodetic studies [Savage and Burford, 1973; Thatcher, 1979; Sauber *et al.*, 1989] suggest that little if any elastic strain accumulates on either side of the CSAF.

[4] Aseismic slip on the CSAF shows several kinds of time dependence. Shallow slip, as measured by surface measurements across the narrow creeping zone, occurs partly as ongoing steady creep, along with brief episodes with slip from mm to cm [e.g., Lisowski and Prescott, 1981]. The depth of these creep events appears to be less than 500 m [Gladwin *et al.*, 1994], with deeper slip thought to be more steady. Creep rates along the San Juan Bautista segment increased after the 1989 Loma Prieta earthquake [e.g., Behr *et al.*, 1997] and slow slip transients of varying duration and magnitude occurred in both transition segments [Linde *et al.*, 1996; Murray and Segall, 2005]. Nadeau and McEvilly [2004] interpret patterns of repeating micro-earthquakes along the CSAF to reflect possible periodic slip-rate variations along the fault. However, over the course of the last 40 years, average surface creep rates have not systematically changed [Titus *et al.*, 2006].

### 2. GPS Data and Analysis

[5] Previous geodetic studies along the CSAF have considered triangulation and EDM (Electronic Distance Measurement) data together with fault slip measurements from creepmeters and alignment arrays [e.g., Thatcher, 1979; Sauber *et al.*, 1989], and more recently GPS measurements [Titus *et al.*, 2006].

[6] During 2003–2005, several surveys were conducted around the creeping segment. Figure 1 shows velocities of these GPS sites, which fill the gap between the well-surveyed San Juan Bautista and Parkfield areas, where there are continuous GPS (CGPS) data from the regional BARD, SCIGN and PBO networks (including 4 sites initially installed by the University of Wisconsin), as well as survey-mode GPS velocities from the BAVU [d'Alessio *et al.*, 2005] and SCEC CMM3 (<http://epicenter.usc.edu/cmm3/>) compilations. We have velocities from 42 campaign

<sup>1</sup>Laboratoire de Tectonique, UMR7072, Université Pierre et Marie Curie, France.

<sup>2</sup>Berkeley Seismological Laboratory, University of California, Berkeley, California, USA.

<sup>3</sup>IGPP, Scripps Institution of Oceanography, University of California, San Diego, La Jolla, California, USA.

<sup>4</sup>U.S. Geological Survey, Menlo Park, California, USA.

<sup>5</sup>Earthquake Research Institute, Tokyo University, Tokyo, Japan.

<sup>6</sup>Department of Geology and Geophysics, University of Wisconsin, Madison, Wisconsin, USA.

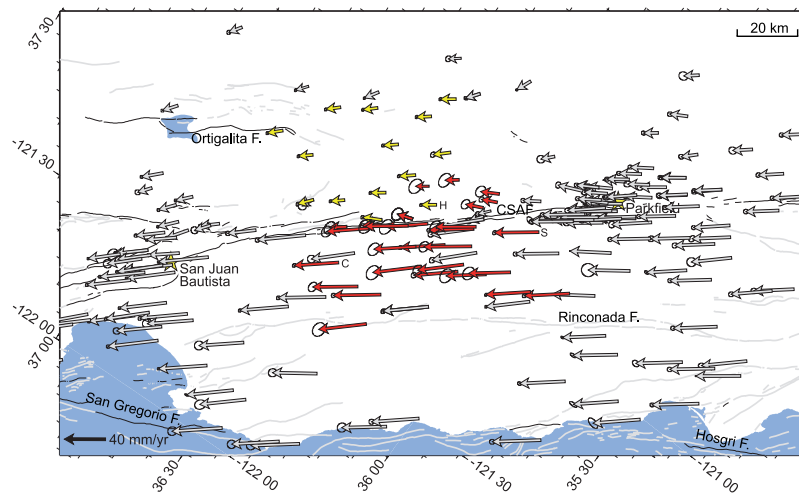


**Figure 1.** Campaign GPS velocities spanning 1991 to 2004 together with GPS data from regional networks (grey) in a North-America fixed reference frame. Yellow (Benito network) and red vectors are our campaign measurements corrected for the local earthquakes as described in the text. The oblique Mercator map projection is about the Pacific Plate-Sierra Nevada/Great Valley pole of rotation. Labeled stations are H, HEPS; C, CHLN; and S, SHAD.

GPS sites not previously available, details on the occupation history of each site are provided in Table S1.<sup>1</sup> We use the GAMIT/GLOBK GPS processing software to analyze the GPS data and to combine our daily solutions and an appropriate set of global and regional solutions from the Scripps Orbital and Permanent Array Center (<http://sopac.ucsd.edu>). We scale the errors following the method used by the SCEC CMM3 analysis with random-walk perturbation to station positions in the Kalman filtering process. Two of our surveys were responses to the 2003 San Simeon and the 2004 Parkfield earthquakes. To account for earthquake-related motions from these earthquakes we used models of coseismic and postseismic slip from *Rolandone et al.* [2006] and *Johanson et al.* [2006] to determine the coseismic and postseismic displacements at each site (Figure S1 and Table S2). Removing the earthquake-related displacements gives an estimate of the interseismic velocity (Figure 1 and Tables S3 and S4).

### 3. Long-Term Deformation

[7] EDM surveys were conducted between some of these sites between 1959 and 1983 [*King et al.*, 1987]. In addition, the Benito network NE of the CSAF was observed using EDM in 1982 [*Sauber et al.*, 1989]. Figure 2 shows the line length changes for two fault crossing lines between 1959 and 2004, combining EDM measurements with the 1998 and 2004 GPS observations. Figure S2 shows the history of 7 other fault-crossing lines. The EDM lengths have been adjusted to be equivalent to GPS, and we applied corrections for offsets from the 1966 Parkfield, 1982 New Idria, 1983 Coalinga/Nunez, 1985 Kettleman Hills, and 2003 San Simeon earthquakes. Table S5 gives the 34 line-length changes for the EDM lines and the earthquake corrections. As Figure 2 shows, the data are matched by a constant rate over the 40-year timespan. Comparison of

line-length changes away from the CSAF in the Benito network also shows no significant differences. Relying on these episodic geodetic data, deformation across the central CSAF has been steady over four decades.

### 4. Kinematics of Aseismic Slip Along the CSAF

[8] To investigate the kinematics of aseismic slip along the CSAF we model the measured velocity field with displacements from rectangular dislocations in an isotropic,

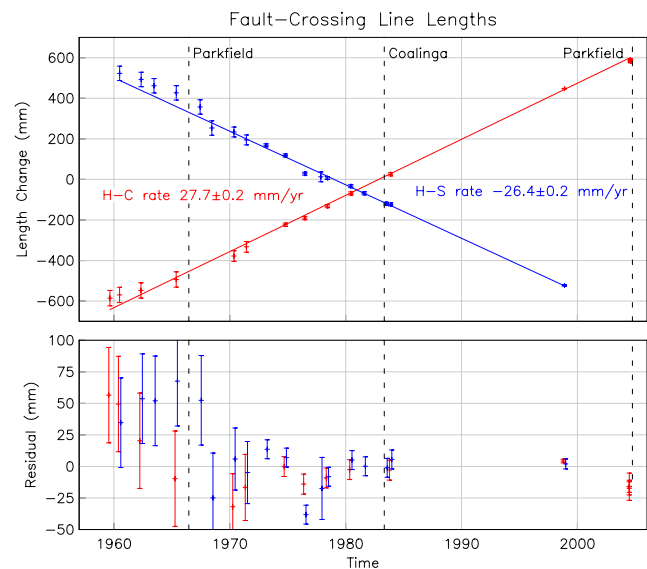


**Figure 2.** (top) Line length changes for two fault crossing lines between 1959 and 2004: H-C, baseline HEPS-CHLN, and H-S, baseline HEPS-SHAD (stations are labeled in Figure 1). Dashed lines show the times of the Parkfield earthquakes of 1966 and 2004, and the 1983 Coalinga earthquake. (bottom) The residuals from a linear fit. The apparent offset in pre-1969 measurements may be due to instrumental differences [*King et al.*, 1987].

<sup>1</sup>Auxiliary materials are available in the HTML. doi:10.1029/2008GL034437.

homogeneous and elastic half-space [Okada, 1985]. The fault is subdivided into a grid of smaller fault elements and we determine the optimal strike-slip rate on each patch. A deep dislocation is included extending below the locking depth to simulate interseismic strain accumulation [Savage and Burford, 1973]. We use one deep dislocation to model the deep creeping zone, providing an estimate of the long-term slip rate of the CSAF. The locking depth is 12 km along the CSAF and 20 km along the Carrizo Plain [d'Alessio et al., 2005]. The fault area above the locking depth is discretized into five shallow dislocations. The strike of the shallow dislocations matches the mapped surface trace of the San Andreas fault (Figure 3b). Table S6 provides the fault model parameters. Our inversion allows us to estimate the optimal slip rate values on the discretized elements that minimize the weighted residual sum of squares with the GPS data. Consideration of a range of model parameterizations suggests that more complex models are not warranted by the distribution and precision of the data.

[9] The distributed slip inversion along the CSAF is shown in Figure 3c, and the residual velocities in Figure 3b. We estimate up to  $28.4 \pm 0.5$  mm/yr of creep in the central creeping section and a  $34.5 \pm 0.5$  mm/yr deep slip rate. Stated uncertainties are formal errors and do not reflect added uncertainties from model parameterization. Increasing the depth of the shallow dislocations to 15 km does not change the shallower creep rates but increases the deep slip rate to 36 mm/yr, with a slightly larger misfit.

[10] Small amounts of right-lateral slip may occur on the Ortigalita fault (about 30 km northeast of the SAF), and the Rinconada and San Gregorio-Hosgri faults (about 25 km and 50 km to the southwest, respectively, as labeled in Figure 1). Our GPS velocity field in the Pacific reference frame (Figure 3a) provides some constraint on the poorly-known offshore deformation. Modeling the San Gregorio-Hosgri fault system using a deep dislocation, we find that it accommodates 4.3 to 5.3 mm/yr of right-lateral slip, depending on slightly different geometries, whereas the Rinconada fault accommodates less than 1 mm/yr. Adding a fault along the eastern margin of the Coast Ranges that extends SE of the Ortigalita fault we find a right-lateral slip rate ranging from 3.8 to 4.2 mm/yr. Considering contributions of strain accumulation on these adjoining faults to the surface deformation, the estimated long-term slip rate of the CSAF varies between 31 and 35 mm/yr.

## 5. Deformation Adjacent to the CSAF

[11] To accentuate the off-fault deformation, Figure 3a shows our GPS velocity field with all the sites on the SW of the CSAF shown with respect to the Pacific plate and those to the NE with respect to the Sierra Nevada Great Valley block, using the poles of rotation from d'Alessio et al. [2005]. The way the velocities swing towards and away from the SAF around Parkfield reflects the transition from creeping to locked conditions, well matched by our model.

[12] We use the program VISR (Velocity Interpolation for Strain Rates) with the interpolation algorithm of Shen et al. [1996], which computes the strain-rate tensor distribution using a weighted average of surrounding GPS velocities. The strain is computed from data on either side of the fault

in order to examine the strain off the SAF. Figure 3a shows the principle axes of strain from our GPS velocities. Adjacent to the creeping segment strain rates are very small, with maximum right-lateral shear less than  $0.083 \pm 0.010$  strain/yr. The strain analysis of the residual velocities from our model (Figure 3b) shows the deformation not accounted for by strike slip on the CSAF. On the NE side of the creeping segment, the contraction rate is  $0.081 \pm 0.016$  strain/yr with the orientation of the most contractional strain at  $N49^\circ E \pm 5^\circ$ , perpendicular to the fault. However, our estimate of total shortening across the Coast Ranges to the NE of the CSAF is highly sensitive to the area being considered, ranging from  $1.5 \pm 0.9$  mm/yr (considering a 30-km-wide, 120-km-long profile centered about Monarch Peak) to  $5.6 \pm 1.2$  mm/yr for a larger area ( $-40$  km to 30 km from MP) that includes two sites with possibly anomalous NE-directed velocities near the CSAF (Figure 3b). The fault-normal velocity profiles including and excluding the possible outliers, near-fault or high-residual sites, are shown in Figure S3. The strain rates are lower ( $\leq 0.04$   $\mu$ strain/yr) on the southwestern crustal block.

## 6. Discussion and Conclusions

[13] While the CSAF accommodates most of the plate boundary deformation in central California, small amounts of right-lateral slip occur on adjoining faults. Consideration of these faults in our models suggests that the San Gregorio-Hosgri fault system accommodates 4.3 to 5.3 mm/yr of right-lateral slip and the Rinconada less than 1 mm/yr. Along the eastern margin of the Coast Ranges, d'Alessio et al. [2005] found  $5.4 \pm 1.0$  mm/yr of right-lateral slip along the Valley Margin deformation zone. We find a slip rate of 3.8 to 4.2 mm/yr on this fault zone; however, the improvement in fit to the data from adding contributions from the Valley Margin and Rinconada fault zones is small. Consideration of contributions from these faults and of a range of plausible transition depths along the SAF suggests that the deep, long-term slip rate of the CSAF is between 31 and 36 mm/yr.

[14] The shallow model creep rate of  $28.4 \pm 0.5$  mm/yr is consistent with the average value of  $28 \pm 2$  reported by Lisowski and Prescott [1981] and confirmed by Titus et al. [2006] from short-range trilateration networks and alignment arrays. Since the deep and shallow slip rates differ by 3–8 mm/yr, even the central creeping section has a slip deficit. Our GPS velocities rule out the possibility that the “missing” creep is distributed over a few-km-wide deformation zone, not captured by the near-field measurements. Alternatively, there may be patches of locked fault at depth even along the central CSAF, whose rupture and associated afterslip could make up the deficit. Finally, the slip deficit may be accommodated by aseismic slip accelerations associated with postseismic relaxation following great earthquakes on the adjoining segments of the SAF [Ben-Zion et al., 1993; Lynch et al., 2003]. Surface creep rates in the transition zones of the CSAF have varied in response to more recent nearby earthquakes [e.g., Simpson et al., 1988; Behr et al., 1997]; however, creep measurements [Titus et al., 2006] and our GPS/EDM comparison indicate overall steady rates along the central creeping segment for at least 40 years.

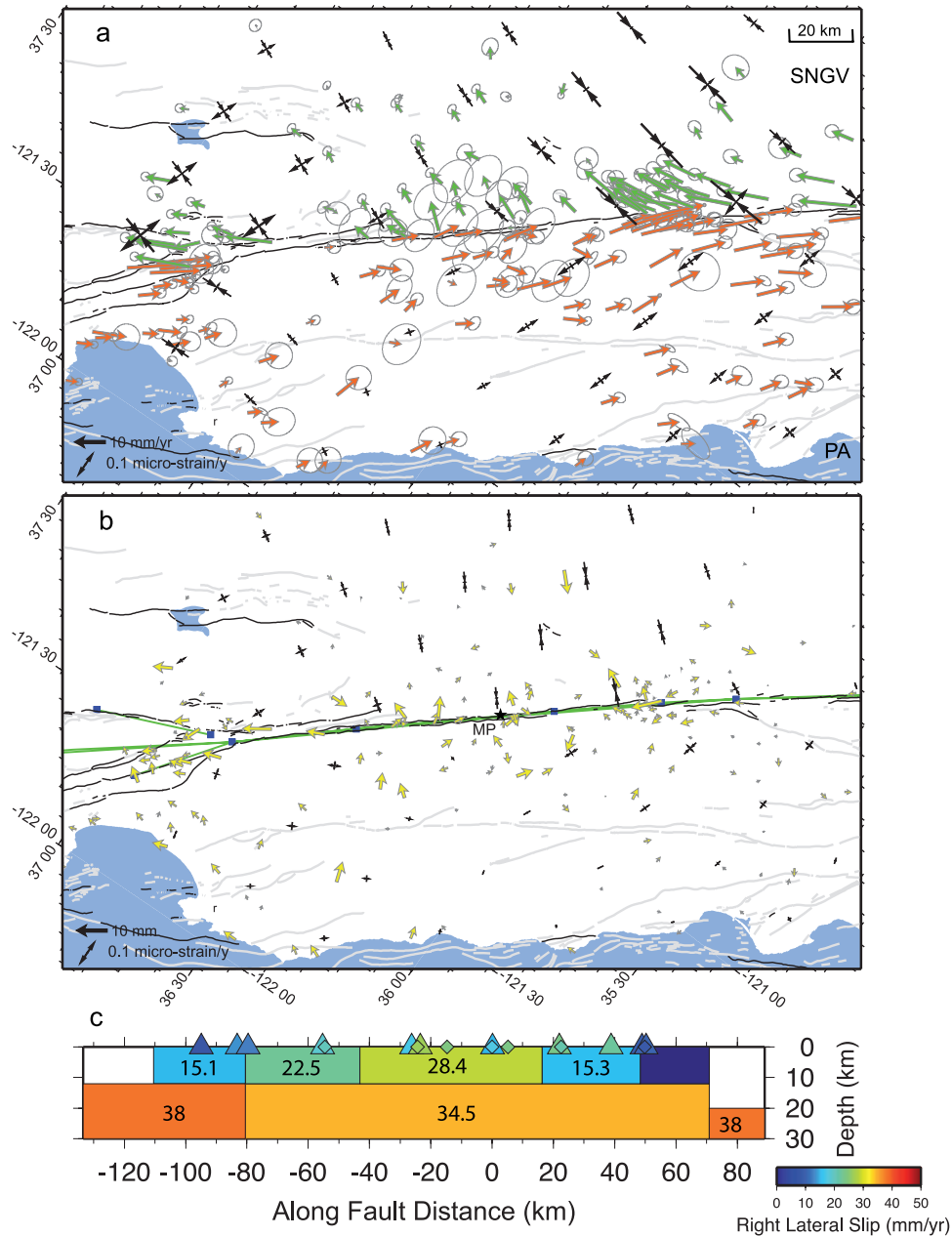


**Figure 3.** Maximum and minimum principal strain rates, measured in  $\mu\text{strain/yr}$ . The strain is computed (a) from the velocities relative to the Sierra Nevada Great Valley block (green) and the Pacific plate (orange) corrected for the local earthquakes as described in the text and (b) from the dislocation-model residual velocities. Green lines show the surface projection of the model dislocations, with the segment end points indicated by dark blue square. (c) Rates of right-lateral strike slip (numbers in mm/yr) for the model inversion for the CSAF. Distance along fault is from Monarch Peak (MP)  $36.21^\circ\text{N}$ ,  $120.79^\circ\text{W}$ . Surface creep rates, from *Schulz et al.* [1982], are shown as colored triangles; colored diamonds show creep rates recorded by alignment arrays from *Titus et al.* [2006].

[15] CSAF-normal convergence is accommodated on contractional structures on both sides of the fault, as evidenced by the occurrence of thrust earthquakes and Late Cenozoic uplift and folding of the Coast Ranges. A recent example is the 2003 Mw 6.5 San Simeon blind-thrust earthquake 50 km W of Parkfield [Rolandone *et al.*, 2006]. The regional strain distribution gives 1–4.5 mm/yr of contraction across the Coast Ranges. *Argus and Gordon* [2001] estimated  $3.2 \pm 1.4$  mm/yr using the projection of the Pacific-Sierra velocity onto the fault-normal direction.

*Sauber et al.* [1989] used triangulation and trilateration data to estimate  $6 \pm 3$  mm/yr of contraction across the 30-km wide San Benito network. Across this network we find a contraction rate of  $0.058 \pm 0.025$  strain/yr from the residual GPS velocities, corresponding to  $1.7 \pm 0.8$  mm/yr of contraction. Geodetic shortening rates are very small ( $1.2 \pm 0.8$  mm/yr) across the Coast Ranges between the CSAF and the Pacific coast. The contrast between the deformation to the NE and SW of the CSAF (Figure 3b) may be related to differences in tectonic evolution, first-

order mechanical properties, geology on the two sides of the fault, and boundary conditions of the plate boundary system [e.g., Page, 1981].

[16] **Acknowledgments.** We thank JPL, USGS, and Caltrans for providing geodetic data. Elements of this work were funded by NSF grants EAR9614774 to USCD, EAR0208038 to UW, and EAR0337308 to UCB. We acknowledge the helpful reviews of Jim Savage and Bob Simpson.

## References

- Argus, D. F., and R. G. Gordon (2001), Present tectonic motion across the Coast Ranges and the San Andreas fault system in central California, *Geol. Soc. Am. Bull.*, *113*, 1580–1592.
- Behr, J., R. Bilham, P. Bodin, K. Breckenridge, and A. G. Sylvester (1997), Increased surface creep rates on the San Andreas fault southeast of the Loma Prieta main shock, *U. S. Geol. Surv. Prof. Pap.*, *1550-D*, 179–192.
- Ben-Zion, Y., J. R. Rice, and R. Dmowska (1993), Interaction of the San Andreas fault creeping segment with adjacent great rupture zones and earthquake recurrence at Parkfield, *J. Geophys. Res.*, *98*, 2135–2144.
- d'Alessio, M. A., I. A. Johanson, R. Bürgmann, D. A. Schmidt, and M. H. Murray (2005), Slicing up the San Francisco Bay area: Block kinematics and fault slip rates from GPS-derived surface velocities, *J. Geophys. Res.*, *110*, B06403, doi:10.1029/2004JB003496.
- Gladwin, M. T., R. L. Gwyther, R. H. G. Hart, and K. S. Breckenridge (1994), Measurements of the strain field associated with episodic creep events on the San Andreas fault at San Juan Bautista, California, *J. Geophys. Res.*, *99*, 4559–4565.
- Johanson, I. A., and R. Bürgmann (2005), Creep and quakes on the northern transition zone of the San Andreas fault from GPS and InSAR data, *Geophys. Res. Lett.*, *32*, L14306, doi:10.1029/2005GL023150.
- Johanson, I. A., E. Fielding, F. Rolandone, and R. Bürgmann (2006), Coseismic and postseismic slip of the 2004 Parkfield earthquake from space-geodetic data, *Bull. Seismol. Soc. Am.*, *96*, S269–S282.
- King, N. E., P. Segall, and W. Prescott (1987), Geodetic measurements near Parkfield, California, 1959–1984, *J. Geophys. Res.*, *92*, 2747–2766.
- Linde, A. T., M. T. Gladwin, M. J. S. Johnston, and R. L. Gwyther (1996), A slow earthquake sequence on the San Andreas fault, *Nature*, *383*, 65–68.
- Lisowski, M., and W. H. Prescott (1981), Short-range distance measurements along the San Andreas fault system in central California, 1975 to 1979, *Bull. Seismol. Soc. Am.*, *71*, 1607–1624.
- Lynch, J. C., R. Bürgmann, M. A. Richards, and R. M. Ferencz (2003), When faults communicate: Viscoelastic coupling and earthquake clustering in a simple two-fault strike-slip system, *Geophys. Res. Lett.*, *30*(6), 1270, doi:10.1029/2002GL016765.
- Murray, J. R., and P. Segall (2005), Spatiotemporal evolution of a slip-rate increase on the San Andreas fault near Parkfield, California, *J. Geophys. Res.*, *110*, B09407, doi:10.1029/2005JB003651.
- Murray, J. R., and J. Langbein (2006), Slip on the San Andreas fault at Parkfield, California over two earthquake cycles and the implications for seismic hazard, *Bull. Seismol. Soc. Am.*, *96*, S283–S303, doi:10.1785/0120050820.
- Nadeau, R. M., and T. V. McEvilly (2004), Periodic pulsing of characteristic microearthquakes on the San Andreas fault, *Science*, *303*, 220–222, doi:10.1126/science.1090353.
- Okada, Y. (1985), Surface deformation due to shear and tensile faults in a half-space, *Bull. Seismol. Soc. Am.*, *75*, 1135–1154.
- Page, B. M. (1981), The southern Coast Ranges, in edited by G. W. Ernst, *The Geotectonic Development of California*, pp. 330–417, Prentice-Hall, Englewood Cliffs, N. J.
- Rolandone, F., D. Dreger, M. Murray, and R. Bürgmann (2006), Coseismic slip distribution of the 2003 Mw 6.6 San Simeon earthquake, California, determined from GPS measurements and seismic waveform data, *Geophys. Res. Lett.*, *33*, L16315, doi:10.1029/2006GL027079.
- Sauber, J., M. Lisowski, and S. C. Solomon (1989), Geodetic measurement of deformation east of the San Andreas fault in central California, in *Slow Deformation and Transmission of Stress in the Earth*, edited by S. C. Cohen and P. Vanicek, pp. 71–86, Vancouver, B. C., Canada.
- Savage, J. C., and R. O. Burford (1973), Geodetic determination of relative plate motion in central California, *J. Geophys. Res.*, *78*, 832–845.
- Schulz, S. S., G. M. Mavko, R. O. Burford, and W. D. Stuart (1982), Long-term fault creep observations in central California, *J. Geophys. Res.*, *87*, 6977–6982.
- Shen, Z. K., D. D. Jackson, and B. X. Ge (1996), Crustal deformation across and beyond the Los Angeles basin, *J. Geophys. Res.*, *101*, 27,957–27,980.
- Simpson, R. W., S. S. Schulz, L. D. Dietz, and R. O. Burford (1988), The response of the creeping parts of the San Andreas fault to earthquakes on nearby faults: Two examples, *Pure Appl. Geophys.*, *126*, 665–685.
- Thatcher, W. (1979), Systematic inversion of geodetic data in central California, *J. Geophys. Res.*, *84*, 2283–2297.
- Titus, S. J., C. DeMets, and B. Tikoff (2006), Thirty-five-year creep rates for the creeping segment of the San Andreas fault and the effects of the 2004 Parkfield earthquake: Constraints from alignment arrays, continuous Global Positioning System, and creepmeters, *Bull. Seismol. Soc. Am.*, *96*, S250–S268, doi:10.1785/0120050811.
- Wesson, R. L., R. O. Burford, and W. L. Ellsworth (1973), Relationship between seismicity, fault creep, and crustal loading along the central San Andreas fault, in *Proceedings of the Conference on Tectonic Problems of the San Andreas Fault System*, edited by R. L. Kovach and A. Nur, *Stanford Univ. Publ. Geol. Sci.*, *12*, 303–321.
- D. C. Agnew, IGPP 0225, University of California, San Diego, La Jolla, CA 92093-0225, USA.
- R. Bürgmann and D. C. Templeton, Berkeley Seismological Laboratory, Berkeley, CA 94720-4760, USA.
- M. A. d'Alessio, Earthquake Research Institute, Tokyo University, Tokyo 113-0032, Japan.
- C. DeMets, B. Tikoff, and S. J. Titus, Department of Geology and Geophysics, University of Wisconsin, Madison, WI 53706, USA.
- I. A. Johanson, U.S. Geological Survey, Menlo Park, CA 94025-3591, USA.
- F. Rolandone, Laboratoire de Tectonique, Université Pierre et Marie Curie - Paris 6, CNRS, 4 place Jussieu, F-75252 Paris, France. (frederique.rolandone@upmc.fr)